ELECTRICAL AND MICROSTRUCTURAL CHARACTERISATION OF MICROCRYSTALLINE SILICON LAYERS AND SOLAR CELLS

Corinne Droz, Evelyne Vallat-Sauvain, Julien Bailat, Luc Feitknecht, Johannes Meier, Xavier Niquille, Arvind Shah
Institute of Microtechnology, University of Neuchâtel, Breguet 2, 2000 Neuchâtel, Switzerland
phone: +41 32 7183200 / fax: +41 32 7183201 / email: corinne.droz@unine.ch

ABSTRACT

This paper attempts to clarify the link between microstructure of hydrogenated microcrystalline silicon (μc-Si:H) and layer transport properties as well as electrical performances of solar cells. Analysis of a series of layers shows that coplanar transport properties in μc-Si:H (as evaluated by σ_{dark}, σ_{photo} and L_{amb}) relate to the size of nanocrystal conglomerates (as observed by TEM and AFM) and not to the average size of individual nanocrystals (as evaluated from XRD). Bifacial Raman crystallinity factors are defined and introduced in order to clarify the relationship between solar cell open-circuit voltage V_{oc} and crystallinity of the top and bottom interface regions. For a variety of nip and pin μc-Si:H solar cells, V_{oc} linearly decreases as the average of the crystallinity factors measured on actual cells increases.

1 INTRODUCTION

Hydrogenated microcrystalline silicon (μc-Si:H) is known to be a complex material consisting of crystalline and amorphous silicon (a-Si:H) phases plus grain boundaries. This material exhibits a wide range of microstructures that depend both on the deposition conditions [1,2] and on the substrate material. At present, the best electrical conversion efficiencies are achieved for μc-Si:H solar cells deposited near the μc-Si:H/a-Si:H transition [3,4], which can be achieved by varying the Silane Concentration $SC = SiH_4/(SiH_4+H_2)$ in the plasma gas phase.

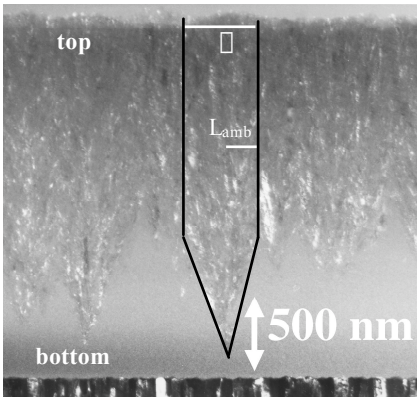

Fig. 1: TEM dark field micrograph of a μc-Si:H layer deposited with SC = 7% on sputtered ZnO. At the bottom of the layer, amorphous silicon appears uniformly grey, between pencil-like conglomerates of nanocrystals (underlined) that constitute the microcrystalline silicon phase. The ambipolar diffusion length (L_{amb}) measured in coplanar geometry and the conglomerate size (□) as measureed from AFM are also indicated.

Indeed, SC used during deposition of the intrinsic layer has been shown to play a significant role in determining the highest attained values of the open-circuit voltage (V_{oc}) in pin cells [5].

The microstructure of μc-Si:H varies not only with SC but also while growth of the film proceeds: a fully amorphous incubation layer has frequently been observed at the bottom of films that are grown close to the μc-Si:H/a-Si:H transition. Thereafter, the microcrystalline phase consists of pencil-like conglomerates made of nanocrystals of a few tens of nanometers size (Fig. 1) [6-8].

This paper is focused on the effect of average nanocrystal sizes (as evaluated from X-Ray Diffraction (XRD)), conglomerate sizes (as evaluated from Transmission Electron Microscopy (TEM) and Atomic Force Microscopy (AFM)) and Raman crystallinity on coplanar transport properties in μc-Si:H layers, as well as on the effect of interface region crystallinity on the V_{oc} of μc-Si:H solar cells.

2 EXPERIMENTAL

2.1. Sample fabrication

Microcrystalline silicon layers and solar cells were deposited by the Very High Frequency Plasma Enhanced Chemical Vapour Deposition (VHF PE-CVD) technique, at a plasma excitation frequency between 70 and 130 MHz and at a substrate deposition temperature of around 220°C. A series of silicon thin films with a thickness of 2.0 - 2.4 μm was deposited on glass substrate at various SC, resulting in intrinsic layers whose microstructure vary from highly microcrystalline (at SC = 5%) to completely amorphous material (at SC = 8%). Solar cells in the nip- and pin-configurations were deposited on glass substrates coated with various types of transparent conducting oxides (Low-Pressure Chemical Vapour Deposited (LP-CVD) Zinc Oxide (ZnO), sputtered ZnO, SnO_2), without any back reflector. In particular, two series of nip cells [6,9] were deposited simultaneously on sputtered ZnO and LP-CVD ZnO, respectively, with constant highly microcrystalline deposition conditions for n- and p- layers. The SC of the i-layers (thickness = 2.0 - 2.5 μm) varied from 5% (highly microcrystalline material) to 7% (mixed μc-Si:H/a-Si:H material). In addition, some other nip cells not pertaining to these series, as well as a large set of pin cells, being typical products of our solar cell technology at IMT Neuchâtel and which cover a wide range of V_{oc} values (see ref. [5]), were also analysed.

2.2. Electrical and microstructural characterisation

The coplanar transport properties of layers were analysed by means of the dark conductivity (σ_{dark}), the

photoconductivity (σ_{photo}) and the ambipolar diffusion length (L_{amb}) within few days after deposition (in order to limit post-oxidation). σ_{photo} and L_{amb}, from which the normalized mobility × lifetime product $\mu\tau/\mu_0\tau_0$ was evaluated [10], were simultaneously measured at room temperature with a Krypton laser (= 647nm) as illumination source and at a generation rate $G \approx 2 \times 10^{19}$ cm^{-3}s^{-1}.

The surface topography of each layer was analysed by AFM in order to evaluate the size of the conglomerates ( ) emerging at the surface. AFM was performed in the non-contact (tapping) mode on a Vista Burleigh Instruments scanning probe microscope.

XRD was used on the layers to calculate the nanocrystal average size with the Scherrer formula from the Full Width at Half Maximum (FWHM) of the (220) peak, see e.g. [1]. XRD was performed on a Philips PW3020 diffractometer, using the Bragg-Brentano geometry (-2 scan) at a wavelength of 1.5418Å.

A few samples from the series of layer and from the series of nip cells were prepared as cross-section sample [6] for TEM observation on a Philips CM200 microscope operated at 200 kV.

2.3. Bifacial depth-dependent micro-Raman technique

A commercial Renishaw Raman Imaging Microscope (System 2000) functioning in backscattering configuration and equipped with a long working-distance objective was operated at two different wavelengths: the strongly-absorbed 514 nm line of an Ar laser and the less-absorbed 633 nm line of a HeNe laser. Bifacial micro-Raman experiments were performed on the layers and on the entire solar cells, i.e. with focused excitation light arriving *either* on the top, last-deposited part of the layer or device (i.e. on the p-layer for the nip devices, and on the n-layer for the pin devices, in both cases through the TCO), *or* on the bottom, first-deposited part of the layer or device, through the glass (and through the TCO in the case of devices). For each layer and each solar cell, both wavelengths were applied in each focusing configuration, resulting in four "bifacial depth-dependent" Raman spectra.

The Raman spectra in the range from 360 to 580 cm^{-1} were then deconvoluted with a quadratic baseline and three Gaussian peaks, attributed to the different phases present in the sample [11]. First, the narrow line centred at about 520 cm^{-1} (which is the position of the TO (Transverse Optic) mode in crystalline silicon (c-Si)) is attributed to silicon crystallites. In our deconvolution procedure, the tail toward smaller wavenumbers is fitted with a peak centred around 510 cm^{-1}, that will be attributed to the defective part of the crystalline phase and therefore included in the crystalline fraction. Finally, a broad peak centred at 480 cm^{-1}, characteristic of the TO mode in a-Si:H, is attributed to the amorphous silicon phase.

The characteristic Raman Collection Depth (RCD) is given by RCD = $1/(2\alpha)$, with α the absorption coefficient of the a-Si:H or c-Si:H material at the considered wavelength, see ref. [12]. RCD ranges from about 50 nm (within a-Si:H) to about 150 nm (within c-Si:H) for the 514 nm excitation light. For the 633 nm excitation light, RCD equals about 500 nm within all the silicon-based layers.

In this work, the "Raman crystallinity factor" σ_c, that is a semi-quantitative value for the crystallinity, is defined as:

$$\sigma_c = (I_c)/(I_c + I_a) \qquad (1)$$

where I_c and I_a are the integrated Raman scattered intensities of the crystalline and amorphous parts, respectively, i.e. $I_c = I_{520} + I_{510}$ and $I_a = I_{480}$. In the expression (1), the ratio of the Raman diffusion cross-sections for c-Si over that of a-Si:H ($y = \sigma_c/\sigma_a$) [13] that should be multiplied with I_a has arbitrarily been set to y = 1; in fact, its actual value is still a matter of debate. The value of σ_c obtained in this manner should be considered as a lower limit for the actual crystalline volume fraction [14].

3 RESULTS AND DISCUSSION

3.1. Layers

In Fig. 2, the different σ_c-values for the SC series of i-layers deposited on glass vary smoothly. The value $\sigma_c \approx 0$ obtained for bottom illumination at 514 nm indicates that the beginning of growth is, for all values of SC, amorphous over a thickness which is at least equal to the corresponding RCD value (≈ 50 nm). The three other curves show a continuous decrease of σ_c with increasing value of SC. The two values of σ_c measured at 633 nm are representative of the bottom (less crystalline) and top (more crystalline) parts of the layer; thereby, the crystallinity within the layers appears to increase as growth proceeds, in agreement with TEM observations (see Fig. 1). The σ_c-value for top illumination at 514 nm is very close to that at 633 nm, indicating that the crystallinity does not change very much in the last hundreds of nanometres of growth of these 2 µm thick layers. We will use thereafter the Raman crystallinity factor σ_c for top illumination at 514 nm as the monitoring parameter instead of the SC value used for i-layer deposition (see Fig. 3).

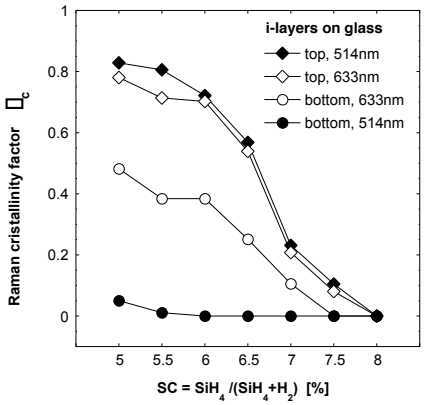

Fig. 2: Raman crystallinity factors (σ_c) (see text) for a series of i-layer (thickness ≈ 2 µm) deposited on glass at various SC. Measurements were performed with =514 nm (filled symbols) and =633 nm (open symbols) excitation light, from the top side (diamonds) and from the bottom side through the glass (circles).

From Fig. 3, $\mu\tau/\mu_0\tau_0$ is lower in the c-Si:H samples than in the a-Si:H ones, while remaining constant as long as c-Si:H material is detected in XRD spectra (i.e. for σ_c between 0.2 and 0.8). On the other hand, the

nanocrystal average size increases roughly linearly with Φ_c. This illustrates, in this series of samples, that coplanar transport is not affected by nanocrystal average size.

Fig. 3 shows that both conglomerate size (□) and L_{amb} slightly decrease with Φ_c for the □c-Si:H samples. Moreover, the ratio L_{amb} / □ is 0.31 - 0.54. From these observations, we can presume that transport is not affected by nanocrystal average size, but rather behaves in accordance with the conglomerate sizes, as already suggested by Kocka et al. [8]. Moreover, the values measured for the dark conductivity prefactor (σ_0) and for the activation energy (E_{act}) agree with the threshold values given in [8].

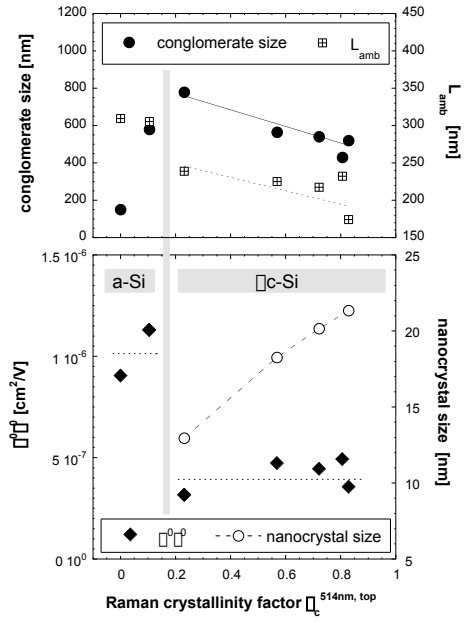

Fig. 3: Top: Conglomerate size (□) evaluated from AFM surface topography (see Fig. 1 for comparison) and ambipolar diffusion length (L_{amb}), with corresponding linear fits; Bottom: mobility □ lifetime product ($\mu\tau$) and nanocrystal size evaluated from the (220) XRD peaks, with guides to the eye, as a function of the Raman crystallinity for a series of silicon layers on glass.

3.2. Solar cells

An effect that is generally observed [4,5] when one increases the SC used for the deposition of the i-layer is a steady increase in the V_{oc}, followed by an abrupt change close to the □c-Si:H/a-Si:H transition. Such a dependence is observed in Fig. 4 for the two nip series.

For the two SC series of nip-type solar cells, on which electrical performances were also measured, the crystallinity was probed with bifacial depth-dependent Raman spectra. For the strongly-absorbed excitation light (514 nm), the collected Raman contribution arises from the doped layer (□20-30 nm) and from the first tens of nanometers of the i-layer. On the other hand, for the weakly-absorbed excitation light (633 nm), the collected Raman contribution arises from about 500 nm below the illuminated surface and, thus, comprises a contribution from the i-layer much larger than that from the doped layer. The values of Φ_c are representative of the bottom n-i (less crystalline) and top p-i (more crystalline) parts of the nip cells; thereby, similarly to i-layers on glass, the crystallinity within the cell appears to increase as growth proceeds. This is confirmed by TEM observations of nip cells [6]: the pencil-like conglomerates of nanocrystals start to grow from the n-layer onwards and are embedded in a-Si:H. The top of the device, consisting of the "last" part of the i-layer plus the p-layer that has grown epitaxially on the underlying i-layer, exhibits a high crystallinity value.

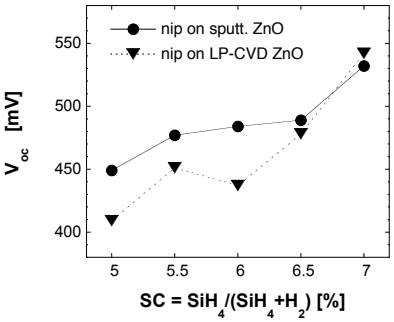

Fig. 4: Open-circuit voltage (V_{oc}) as a function of the SC at which the i-layer has been deposited for two series of nip solar cells, deposited on sputtered ZnO and LP-CVD ZnO, respectively.

In order to evaluate the influence of the crystallinity on the solar cells V_{oc}, we studied the dependence of the V_{oc} on the Φ_c-values measured from the p-i (top) side and n-i (bottom) side for the two SC nip-cell series. Moreover, we introduce here the algebraic average Φ_c^A of the Raman crystallinity factors, that is calculated as follows, for each wavelength:

$$\Phi_c^A = (\Phi_c^{top} + \Phi_c^{bottom})/2 \qquad (2)$$

Fig. 5 illustrates that when Φ_c^A is used as monitor of the device material, a **linear dependence of V_{oc} with Φ_c^A is observed**. In order to confirm this observation, a large set of different solar cells deposited in the nip- and pin-configurations in our laboratory were characterised. Fig. 5 shows that for all the cells analysed, the linear increase in V_{oc} with a decrease in Φ_c^A is confirmed. Note that even if Φ_c is evaluated with a value for the Raman cross-section ratio different from one, the trend observed in Fig. 5 is practically conserved [11]. We have thus shown that Φ_c^A is a parameter simply linked to V_{oc} (Fig. 5), in a better way than SC traditionally used (Fig. 4).

A similar link between V_{oc} and Raman crystallinity has been reported by Klein et al. [15] for some pin cells (V_{oc} = 520-600 mV) with the i-layer deposited by Hot-Wire (HW). However, in that case, the Raman measurements on the cells are performed only from the top side and that after removing the (a-Si:H) n-layer.

In its definition and in the way Φ_c^A is measured, it includes the respective contributions of the doped and undoped layers crystallinities. Highly crystalline p-doped layers have been shown to be beneficial for the electrical performances in pin solar cells [16], as they act as seeding layer for the microcrystalline growth of the i-layer, and as they can be very effectively doped, a feature that is a pre-condition for obtaining a high value of V_{oc}. On the other hand, the n-i interface

contributes also to the internal field in open-circuit conditions and cannot be neglected.

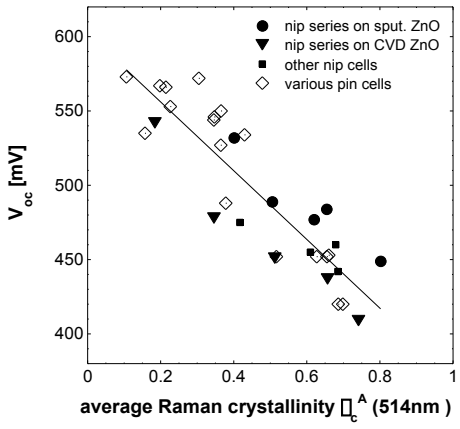

Fig. 5: Dependence of the open-circuit voltage (V_{oc}) of two SC series, as well as of various other nip and of pin □c-Si:H solar cells on the average Raman crystallinity factor ($□_c^A$) (see text) measured at 514 nm. The full line is a linear fit to all the data (nip and pin).

$□_c^A$ takes into account the effect of both n-i and p-i junctions by averaging the crystallinity of the top and bottom parts. From our measurements it becomes clear that both interface regions play an decisive role on V_{oc}, and that it is the average crystallinity (factor) of the two interface regions that counts (see Fig. 5): the more amorphous-like these two interface regions are, on an average, the higher V_{oc} becomes. As the bulk of the i-layer also changes in crystallinity if SC is varied, we are, however, not yet able to say whether it is solely the interface region, as other experiments have suggested [17], or bulk material, as proposed in [18], that determine V_{oc}. To be able to discriminate here, further experiments are necessary.

4 CONCLUSIONS

Electrical performances have been studied in relation with selected microstructural parameters evaluated on □c-Si:H layers and solar cells deposited by PE-CVD. Coplanar transport measurements on a silane concentration series of layers on glass substrate show that the normalized mobility □ lifetime product □'□' relates to the size of nanocrystal conglomerates as observed by AFM rather than to average size of the individual nanocrystals as evaluated from XRD. Moreover, the ambipolar diffusion length measured in these samples equals, in average, half of the diameter of conglomerate. These experimental observations indicate that coplanar transport in □c-Si:H is limited by the defective material present at the conglomerate boundaries.

Bifacial micro-Raman spectroscopy has been carried out on entire single junction □c-Si:H solar cells, on which electrical performances were also measured: this non-destructive and fast technique can be applied for monitoring the crystallinity from the top and bottom sides at various depths in the device. We have identified the algebraic average of the two Raman crystallinity factors ($□_c^A$), which probe the regions close to the n-i and p-i interfaces, as constituting a fundamental microstructural parameter for solar cell device characterisation. Indeed, V_{oc} linearly decreases when $□_c^A$ increases. This has been observed for a large set of solar cells representative of our in-house VHF-PECVD based nip and pin solar cell technologies. Nevertheless, further investigations are needed in order to identify more accurately the precise thickness of the solar cell region that is important for forming V_{oc}.

ACKNOWLEDGEMENTS

This work was supported by the Swiss National Science Foundation under grant FN66985, as well as by the Swiss Federal Office of Energy (OFEN) under contract No. 36487.

REFERENCES

[1] E. Vallat-Sauvain, U. Kroll, J. Meier, A. Shah, J. Pohl, *J. Appl. Phys.* **87**/6**,** 3137 (2000).
[2] M. Luysberg, P. Hapke, R. Carius, F. Finger, *Phil. Mag.* **A 75,** 31 (1997).
[3] A. Shah, J. Meier, E. Vallat-Sauvain, C. Droz, U. Kroll, N. Wyrsch, J. Guillet, U. Graf, *Thin Solid Films* **403,** 179 (2002).
[4] T. Roschek, T. Repmann, J. Muller, B. Rech, H. Wagner, *J. Vac. Sci. Technol. A* **20**/2**,** 492 (2002).
[5] J. Meier, E. Vallat-Sauvain, S. Dubail, U. Kroll, J. Dubail, S. Golay, L. Feitknecht, P. Torres, S. Faÿ, D. Fischer, A. Shah, *Sol. En. Mat. and Sol. Cells* **66,** 73 (2001).
[6] J. Bailat, E. Vallat-Sauvain, L. Feitknecht, C. Droz, A. Shah, *J. Appl. Phys.***,** accepted for publication (2003).
[7] L. Houben, C. Scholten, M. Luysberg, O. Vetterl, F. Finger, R. Carius, *J. Non-Cryst. Solids* **299-302,** 1189 (2002).
[8] J. Kocka, H. Stuchlikova, J. Stuchlik, B. Rezek, T. Mates, V. Svrcek, P. Fojtik, I. Pelant, A. Fejfar, *J. Non-Cryst. Solids* **299-302,** 355 (2002).
[9] L. Feitknecht, O. Kluth, Y. Ziegler, X. Niquille, P. Torres, J. Meier, N. Wyrsch, A. Shah, *Sol. En. Mat. and Sol. Cells* **66,** 397 (2001).
[10] N. Beck, N. Wyrsch, C. Hof, A. Shah, *J. Appl. Phys.* **79**/12**,** 9361 (1996).
[11] C. Droz, E. Vallat-Sauvain, J. Bailat, L. Feitknecht, J. Meier, A. Shah, *submitted to Sol. En. Mat. and Sol. Cells* (2003).
[12] N. Beck, J. Meier, J. Fric, Z. Remes, A. Poruba, R. Flückiger, J. Pohl, A. Shah, M. Vanecek, *J. Non-Cryst. Solids* **198-200,** 903 (1996).
[13] R. Tsu, J. Gonzalez-Hernandez, S. S. Chao, S. C. Lee, K. Tanaka, *Appl. Phys. Lett.* **40**/6**,** 534 (1982).
[14] L. Houben, M. Luysberg, P. Hapke, R. Carius, F. Finger, H. Wagner, *Phil. Mag.* **A 77**/6**,** 1447 (1998).
[15] S. Klein, F. Finger, R. Carius, T. Dylla, B. Rech, M. Grimm, L. Houben, M. Stutzmann, *Thin Solid Films***,** in press (2003).
[16] E. Vallat-Sauvain, S. Faÿ, S. Dubail, J. Meier, J. Bailat, U. Kroll, A. Shah, *Mat. Res. Soc. Symp. Proc.* **664,** A15.3.1 (2001).
[17] J. Meier, S. Dubail, J. Cuperus, U. Kroll, R. Platz, P. Torres, J. A. A. Selvan, P. Pernet, N. Beck, N. P. Vaucher, C. Hof, D. Fischer, H. Keppner, A. Shah, *J. Non-Cryst. Solids* **227-230,** 1250 (1998).
[18] O. Vetterl, A. Lambertz, A. Dasgupta, F. Finger, B. Rech, O. Kluth, H. Wagner, *Sol. En. Mat. and Sol. Cells* **66**/1-4**,** 345 (2001).